Real-Time Emulator for Reproducing Graded Potentials in Vertebrate Retina

Hirotsugu Okuno, Jun Hasegawa, Tadashi Sanada, and Tetsuya Yagi

***Abstract*—In most parts of the retina, neuronal circuits process visual signals represented by slowly changing membrane potentials, or so-called graded potentials. A feasible approach to speculate about the functional roles of retinal neuronal circuits is to reproduce the graded potentials of retinal neurons in response to natural scenes. In this study, we developed a simulation platform for reproducing graded potentials with the following features: real-time reproduction of retinal neural activities in response to natural scenes, a configurable model structure, and compact hardware. The spatio-temporal properties of neurons were emulated efficiently by a mixed analog-digital architecture that consisted of analog resistive networks and a field-programmable gate array. The neural activities on sustained and transient pathways were emulated from 128 × 128 inputs at 200 frames per second.**

***Index Terms*—Emulation, graded potential, neuromorphic, retina.**

I. Introduction

THE vertebrate retina is a type of neural tissue that performs light detection as well as visual preprocessing prior to perceptual processes in the brain. In most parts of the retina, except for particular types of neurons including ganglion cells, signals are represented by slowly changing membrane potentials called graded potentials ([1], [2], see also [3] for an overview). The slow time course of these potentials originates from the phototransduction process, which occurs in photoreceptors and is the first stage of processing in the retina (see [4] for a review). The graded voltage signals generated by photoreceptors [2] are fed into the first neuronal network of the retina [5], called the outer retinal network (ORN), in the outer plexiform layer (OPL). The outputs of the ORN are further fed into the second neuronal network of the retina, known as the inner retinal network, in the inner plexiform layer (IPL). In these networks, multiple sub-circuits, e.g., on-type and off-type circuits, are embedded in parallel, and each sub-circuit applies particular spatio-temporal filters to enhance or extract particular visual information (see [3], [6] for overviews). Because most of the neurons in these circuits use graded potentials, investigating their spatio-temporal distributions, i.e., their neural images, within the retinal circuit is necessary for understanding the functional roles of individual sub-circuits.

Although longstanding physiological and anatomical observations have revealed the typical response properties of retinal neurons and their underlying circuit structures, there are three reasons why understanding the functional role of these neurons under natural conditions is not straightforward. First, the images received by the retina under natural conditions are far more complex spatio-temporally than those used in physiological experiments (e.g., spots, gratings, and randomized checker boards). Second, the number of neurons recorded simultaneously is limited to a small number owing to technical difficulties, whereas a large number of neurons could code a particular type of visual information. Third, eye movements must be taken into account because the retina receives images under a strong influence of movement.

One of the most feasible approaches to overcome these difficulties is reproducing the neural activities suggested by physiological and/or anatomical observations (e.g., [7], [8], [9], [10]) and elucidating the relationship between input images including natural scenes and reproduced neural images under realistic illumination conditions. In this regard, a simulation platform with the following features is required: real-time reproduction of neural images in response to natural scenes, a configurable model structure that performs parallel processing of graded potentials, and compact hardware to be installed on a mock-up system that can reproduce eye movements.

In terms of these requirements, conventional fully digital computing systems based on sequential processing are ill-suited for the simulation platform above because the costs of performing the computations with compact hardware in real time are too high. This high computational cost stems from the fact that simulating the receptive fields of retinal neurons requires a large two-dimensional digital spatial filter, which includes a large number of product-sum operations. Consequently, fully digital systems inevitably require a powerful large-scale platform.

An alternative way to reproduce neural images is to employ so-called silicon retinas, which are analog very large scale integrated (VLSI) vision sensors with image processing circuits that imitate the fundamental structures of retinal circuits [11], [12] (see also [13], [14] for overviews). The high computational efficiency of these retinas enables them to mimic the responses of retinal neurons in real time with compact hardware in a natural visual environment. Early silicon retinas were fabricated to imitate circuit structures in the OPL of the vertebrate retina [11], [15], [16], [17]. The designs for silicon retinas have been extended to include a part of the IPL [18], [19], [20], the primary

Manuscript received November 24, 2013; revised February 16, 2014; accepted April 29, 2014. This work was supported by Challenging Exploratory Research (24650314) from The Ministry of Education, Culture, Sports, Science and Technology. This paper was recommended by Associate Editor J. Van der Spiegel.

The authors are with Osaka University, Suita, Osaka 565-0871, Japan (e-mail: h-okuno@eei.eng.osaka-u.ac.jp).

This paper has supplementary downloadable material available at http://ieee-explore.ieee.org.

Digital Object Identifier 10.1109/TBCAS.2014.2327103

visual cortex [21], or other specific functions [22], [23], [24], [25], [26]. Practical applications that take advantages of silicon retinas have also been proposed [27], [28], [29], [30].

These silicon retinas simulate the spatial response properties of retinal neurons instantaneously by taking advantage of their built-in analog circuits with continuous sampling sensors. However, these features can be shortcomings when reconstructing the graded potentials of retinal neurons. Semiconductor integrated circuits require a large space to implement a long time constant of biological circuits. In addition, built-in analog circuits have difficulty modifying the process flow and configuring the parameters required for neural simulations.

To achieve an appropriate platform for simulating retinal circuits, an analog-digital mixed architecture that combines a silicon retina with a personal computer (PC) has been proposed [31], [32]. The silicon retina used in these studies samples images in a frame-based manner and applies a spatial filter to the frame-based image instantaneously by using built-in analog circuits that imitate neuronal circuits in the OPL [33]. Graded potentials with an appropriate time constant were reproduced in the PC by applying temporal digital filters to the frame-based data. The proposed system demonstrated on-line and real-time reproduction of neural images of the OPL in response to natural scenes, although its frame sampling rate (62.5 frames/s) was inadequate for precise reproduction of neural images and the PC-containing system was not sufficiently compact.

The aim of this study is to develop a high-speed, compact, and configurable retina emulator, using a built-in analog circuit and reconfigurable digital circuits in their appropriate roles. Built-in analog circuits were used to imitate the spatial connectivity of photoreceptors [34] and horizontal cells [35]. By contrast, simulating the IPL requires extensibility because a large part of the circuit remains under investigation; hence, reconfigurable circuits were used to simulate the IPL. All temporal properties were simulated by digital filters. Computations that employed image data sampled at a high frame rate (200 frames/s) achieved real-time reproduction of retinal neuronal images without degrading the dynamic features of the graded potentials of retinal neurons.

II. Retina Emulator

A. Hardware Architecture

We developed a retina emulator by using an analog-digital-mixed image sensor system, which is mainly composed of a silicon retina (ASPECTUS-U, Neuralimage Co., Ltd), a field-programmable gate array (FPGA: Xilinx SC3S400), and a universal serial bus (USB) interface (Cypress CY7C68013A) (Fig. 1). The photographs in Fig. 2 show the appearance of the emulator with and without a metal chassis and a lens.

The silicon retina used here is an analog VLSI image sensor with image processing circuits. The design of a pixel is essentially the same as that described in [33]. It has 128×128 pixels, each of which consists of an active pixel sensor (APS), two sample/hold amplifiers, and two layers of resistive networks. Each pixel is connected to four neighboring pixels in each layer of the resistive network that functions as a spatial smoothing filter. The design of the resistive network is described in [36].

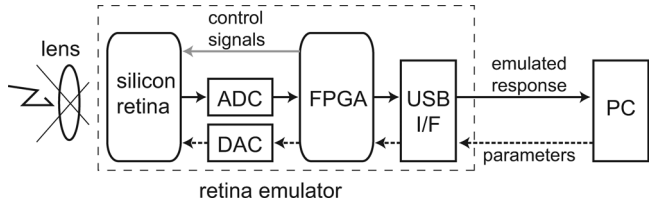

Fig. 1. Diagram of the system structure. The emulator consists of a silicon retina, an FPGA, signal converters, and a USB interface. A PC is used for receiving the output data and for configuring the parameters.

Fig. 2. Appearance of the retina emulator. (a) Emulator with a metal chassis and a lens. (b) Inside of the metal chassis.

The silicon retina receives visual inputs through an optical lens with a diaphragm assembly (maximum f-number: 1.4). The visual signal processed by the silicon retina is transmitted to the FPGA via an 8-bit analog-to-digital converter (ADC) at 200 frames per second and stored in a memory. The stored image data are expressed by fixed-point 12-bit values in the FPGA. These data are further processed in the FPGA and passed to the USB interface, which then transfers the processed data to a PC from which it receives the parameter settings for emulating neural activity.

B. Signal Process Flow

The retina emulator reproduces the essence of the computations carried out in biological retinal circuits in real time by taking advantage of both analog and digital circuits.

Fig. 3 depicts a computational model that reflects the OPL neuronal circuitry. In this figure, blocks $\mathrm{TF_p}$ and $\mathrm{TF_h}$ represent the temporal properties of a photoreceptor and a horizontal cell, respectively. Blocks $\mathrm{TF_{b1}}$ and $\mathrm{TF_{b0}}$ represent the temporal properties of an on-center bipolar cell and an off-center bipolar cell, respectively [5], [37]. Blocks $\mathrm{SF_p}$ and $\mathrm{SF_h}$ represent the spatial properties mediated by the gap junction networks of cone photoreceptors [34] and horizontal cells [35], respectively. Unlike the IPL, in which visual signals are modified by various types of amacrine cells in many different ways, the gap junction network of the OPL can be simply modeled as a resistive network [34], [35]; hence, resistive networks were employed to mimic the spatial property of the OPL efficiently. Despite the compact hardware, the resistive network instantaneously performs large-scale spatial filtering, which would be computationally costly for conventional digital systems to emulate.

Fig. 4 depicts the process flow of the retina emulator. Assuming that the spatial and temporal filters in Fig. 3 are simu-

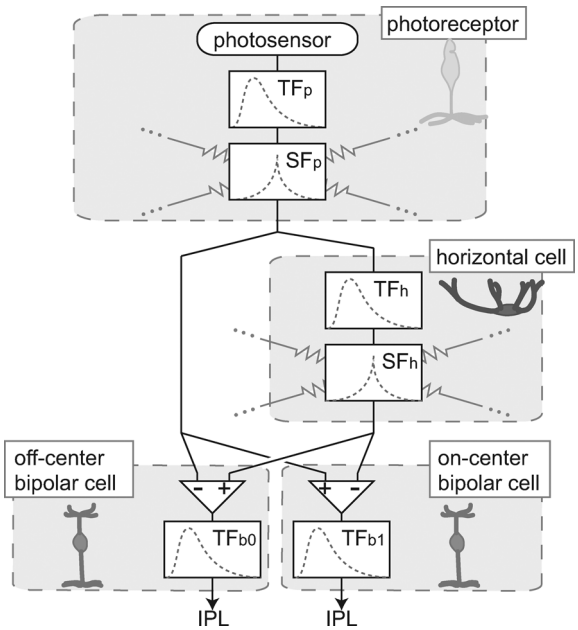

Fig. 3. Computational model that reflects the neuronal circuitry of the outer plexiform layer (OPL). Blocks $\mathrm{TF_p}$, $\mathrm{TF_h}$, $\mathrm{TF_{b1}}$, and $\mathrm{TF_{b0}}$ represent the temporal properties of a photoreceptor, a horizontal cell, an on-center bipolar cell, and an off-center bipolar cell, respectively. Blocks $\mathrm{SF_p}$ and $\mathrm{SF_h}$ represent spatial properties mediated by the gap junction networks of photoreceptors and horizontal cells, respectively.

lated by linear filters [38], [39], the order of the blocks in Fig. 3 is interchangeable. By changing the order of computation, all temporal properties of neurons in the OPL and IPL were simulated in the FPGA, as shown in Fig. 4, because digital circuits are more suitable for accurate simulation of their temporal properties with a long time constant.

The role of block TF1 in Fig. 4 is to simulate the delay of the lateral inhibition mediated by horizontal cells. Blocks TF2 and TF3 reflect the temporal properties of both a photoreceptor ($\mathrm{TF_p}$ in Fig. 3) and a bipolar cell ($\mathrm{TF_{b1}}$, $\mathrm{TF_{b0}}$ in Fig. 3). The output signals of these filters (b_1, b_0) represent the responses of on-center and off-center bipolar cells, respectively. Blocks SF1 and TF4 (surrounded by the dashed lines) represent spatial and temporal low-pass filters, respectively. In the salamander retina, neurons mediating this spatio-temporal low-pass filtering are considered to be narrow-field amacrine cells [7]. The output signal of these low-pass filters ($a_{1\mathrm{T}}$, $a_{0\mathrm{T}}$) is subtracted from the bipolar cell response and rectified. This rectification (RECT in Fig. 4) simulates the limited hyperpolarization of a particular type of amacrine cell whose resting potential is low. Although more sophisticated nonlinear functions should be used to implement this contribution, here we employed a simple rectifier for convenience. By assigning spatial and temporal computations to the most suitable processing devices, this emulator efficiently reconstructs the retinal neural responses.

In addition to the temporal properties of the OPL, those of the IPL are also emulated by the FPGA. All temporal filters implemented in the FPGA use infinite impulse response (IIR) filters to reduce memory usage. Each temporal filter represents the temporal properties of both the synaptic connection and the membrane potential.

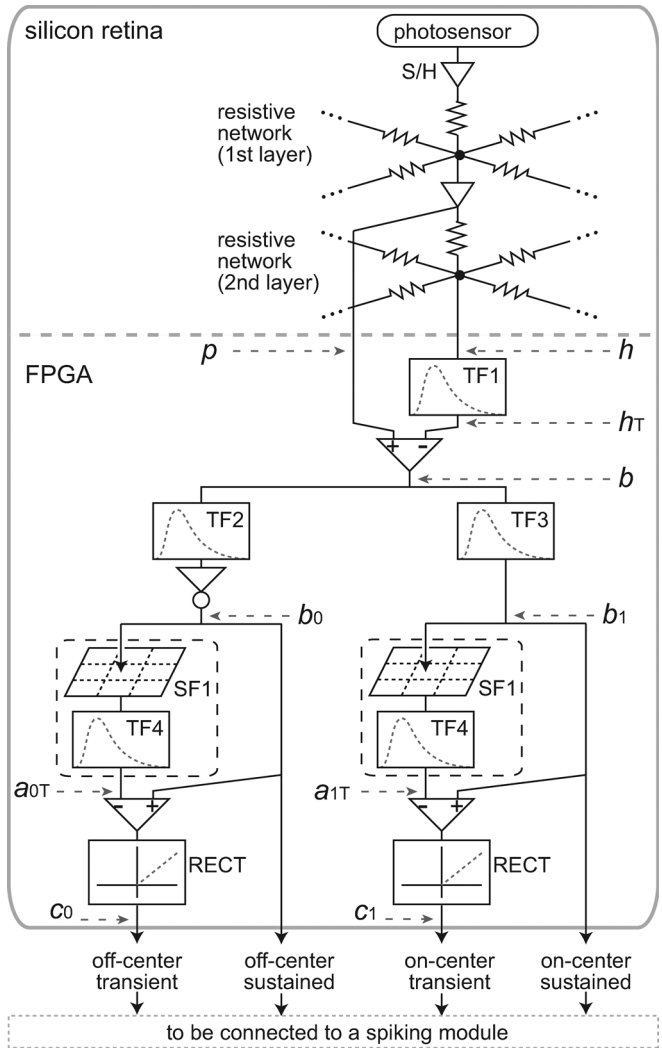

Fig. 4. Process flow diagram of the retina emulator. The spatial property of the OPL is emulated by two resistive network layers in the silicon retina. The temporal properties of both the OPL and IPL are emulated by the FPGA. All temporal filters (TF1, TF2, TF3, and TF4) implemented in the FPGA use IIR filters to reduce memory usage. See text for details.

The spatial properties of the IPL are emulated by the FPGA. Because of the various forms of spatial processing mediated by a wide variety of amacrine cells, using built-in analog circuits to emulate the spatial properties of the IPL is inappropriate. In contrast, the parallel and configurable spatial processing provided by FPGAs is suitable for this purpose. Although the spatial filtering implemented here emulates only a simple diffusion process mainly mediated by narrow-field amacrine cells, more realistic spatial properties could be added easily by implementing additional circuits in the FPGA.

C. Emulating Spatio-Temporal Processing of the OPL

The spatial smoothing function mediated by the gap junctions of the photoreceptors and horizontal cells are emulated by the first and second layers, respectively, of the resistive network in the silicon retina. The width of the smoothing filter, i.e., the degree of exponential decay of the smoothed image, can be easily controlled by an externally applied voltage to the resisters because the resistive network of the silicon retina is implemented

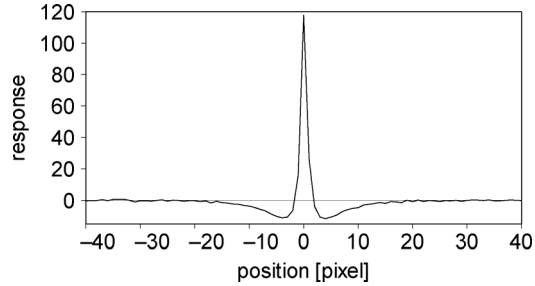

Fig. 5. Difference between the spatial impulse responses of the first and second resistive networks. This spatial property reproduces that of bipolar cells.

with metal-oxide-semiconductor (MOS) transistors [11]. The design of the present MOS resistor is described in [36].

Fig. 5 shows the difference between the spatial impulse responses of the first and second resistive networks. The plot exhibits the center-surround antagonistic property just as does the spatial property of bipolar cells. The smoothed images obtained by the resistive networks are fed into the FPGA after being digitized by an 8-bit ADC. In Fig. 4, the signals sent from the first and second layers are denoted as p and h, respectively.

A first-order IIR filter is applied to h, simulating the delay of lateral inhibition (TF1 in Fig. 4). The filtered signal is expressed as

$$h_{\mathrm{T}}[x, y, i] = \alpha h[x, y, i] + (1 - \alpha) h_{\mathrm{T}}[x, y, i - 1] \qquad (1)$$

where α ($0 < \alpha < 1$) represents a configurable parameter that determines the time constant of the delay of lateral inhibition.

The center-surround antagonistic property of the bipolar cell is obtained by the difference between p and h_{T}.

$$b[x, y, i] = p[x, y, i] - h_{\mathrm{T}}[x, y, i] + v_r \qquad (2)$$

where v_r ($= 128$) represents the resting potential. Actual retinal bipolar cells can be classified in terms of their response polarity: depolarizing cells, which form the on-center pathway; and hyperpolarizing cells, which form the off-center pathway. To emulate these two pathways, the bipolar cell response bifurcates into two pathways, and a temporal filter that simulates the temporal response of either of an on-center or off-center bipolar cell is applied to signal b. These temporal filters (TF2 and TF3 in Fig. 4) are formed by the following four IIR filters:

$$b_{\mathrm{Tn}}[x, y, i] = \beta_n b[x, y, i] + (1 - \beta_n) b_{\mathrm{Tn}}[x, y, i - 1] \qquad (3)$$

where n (n = 1, 2, 3, 4) indicates the index of the IIR filter, and β_n represents a configurable parameter that determines the time constant of that filter. The simulated responses of on-center (b_1) and off-center (b_0) bipolar cells are given by the linear summation of thes following four IIR filters:

$$b_1 = k_1 b_{\mathrm{T1}} + k_2 b_{\mathrm{T2}} + k_3 b_{\mathrm{T3}} + k_4 b_{\mathrm{T4}} \qquad (4)$$

$$b_0 = -(l_1 b_{\mathrm{T1}} + l_2 b_{\mathrm{T2}} + l_3 b_{\mathrm{T3}} + l_4 b_{\mathrm{T4}}) + v_r. \qquad (5)$$

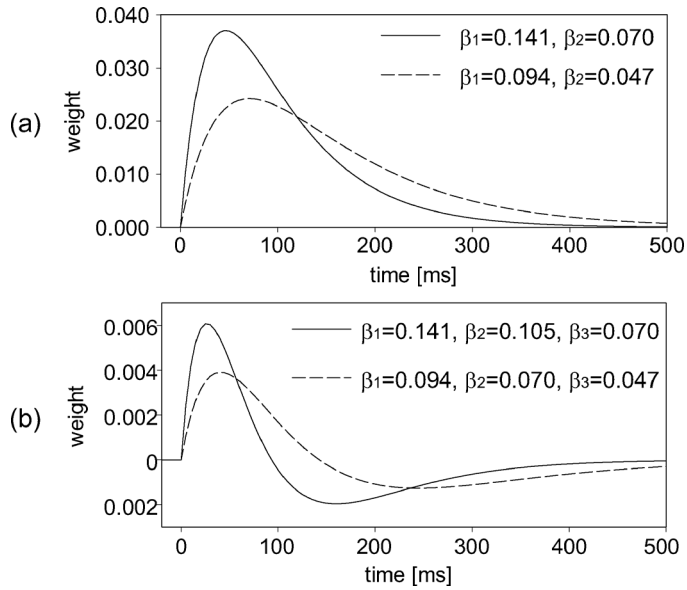

Fig. 6. Examples of unit impulse response of a bipolar cell. Parameters (k_1, k_2, k_3, k_4) are set to (a) $(-1, 2, 0, 0)$ or (b) $(-1, 2, -1, 0)$.

Coefficients k_n and l_n determine the time course of on-center and off-center cell responses, respectively. Fig. 6(a) and (b) shows examples of the unit impulse response with particular sets of parameters. With four IIR filters, various temporal filters can be formed for both on-center and off-center bipolar cells to conserve memory.

D. Emulating Spatio-Temporal Processing of the IPL

The visual signal processed in the OPL is transmitted by either the on-center or off-center bipolar cell to the IPL, where neuronal sub-circuits mediated by various types of amacrine cells have been found. In this study, a single spatio-temporal processing that imitates signal diffusion mediated by narrow-field amacrine cells was implemented. Although the signal processing on the on-center pathway is explained in this subsection, the computations are essentially the same on the off-center pathway.

Fig. 7 shows the signal flow for emulating the spatio-temporal processing of amacrine cell responses. Each simulated amacrine cell receives signals from a bipolar cell at the same retinal position and adjacent amacrine cells; the signal received by an amacrine cell is expressed as

$$a_{1\mathrm{S}}[x, y, i] = G_{\mathrm{b}} b_1[x, y, i] + G_{\mathrm{a}} \sum_{(\mathrm{p},q) \in M_{\mathrm{adj}}} a_{1\mathrm{T}}[p, q, i - 1] \qquad (6)$$

where G_{b} denotes the bipolar-amacrine gain, G_{a} denotes the amacrine-amacrine gain, and M_{adj} represents the adjacent eight pixels. The simulated amacrine cell response is updated by using an IIR filter in accordance with the following equation:

$$a_{1\mathrm{T}}[x, y, i] = \gamma a_{1\mathrm{S}}[x, y, i] + (1 - \gamma) a_{1\mathrm{T}}[x, y, i - 1] \qquad (7)$$

where γ ($0 < \gamma < 1$) denotes a configurable parameter that determines the temporal property of the amacrine cell.

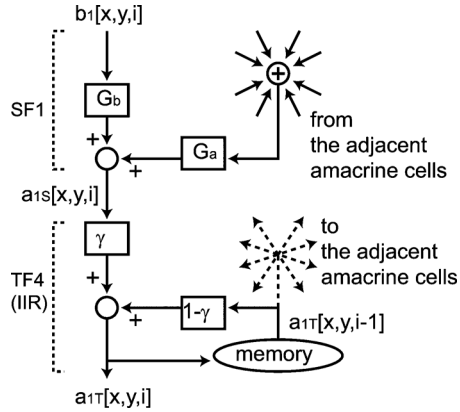

Fig. 7. Process flow diagram for simulating the spatio-temporal filtering of narrow-field amacrine cells.

TABLE I
PARAMETERS

region	parameter	range	values used
OPL	L_1	0.9 to 7.9	0.9
	L_2	0.9 to 12.6	12.6
	α	0 to 1	0.258
	$(\beta_1, \beta_2, \beta_3, \beta_4)$	0 to 1	(0.094, 0.047, 0, 0)
	(k_1, k_2, k_3, k_4)	arbitrary	(-1, 2, 0, 0)
	(l_1, l_2, l_3, l_4)	arbitrary	(-1, 2, 0, 0)
	(θ_1, θ_0)	-128 to 127	(0, 0)
IPL	G_a	0 to 1	0.531
	G_b	0 to 0.125	0.063
	γ	0 to 1	0.063

This amacrine cell response inhibits the bipolar cell response, resulting in a transient-type response observed in particular cells in the IPL [7] (e.g., wide-field amacrine cells)

$$c_1 = \begin{cases} b_1 - a_{1\mathrm{T}} & (b_1 - a_{1\mathrm{T}} > \theta_1) \\ 0 & (b_1 - a_{1\mathrm{T}} \leq \theta_1). \end{cases} \tag{8}$$

E. Emulated Values and Emulation Parameters

The emulated values obtained from the equations expressed above must be rescaled appropriately so that they represent feasible membrane potentials of a particular neuron. However, in this paper, the values were not rescaled, and calculated values were shown directly.

All emulation parameters are summarized in Table I. Parameters L_1 and L_2 denote the length constants, which are the lengths for the voltage to decrease to 1/e of the maximum, in pixels of the first and second layers of the resistive network, respectively. The value of L_2 is inevitably higher than that of L_1. Parameter θ_0 denotes the threshold in (8) for the off-center pathway.

III. FPGA IMPLEMENTATION

Fig. 8(a) shows the block diagram of digital circuits synthesized in the FPGA. The FPGA reads the image data stored in the sample-and-hold circuits (S/H in Fig. 4) twice because only one of signals p and h can be read at a time. After all the pixel data of signal h are read through the second layer of the resistive network, the pixel data of signal p are read from the first layer.

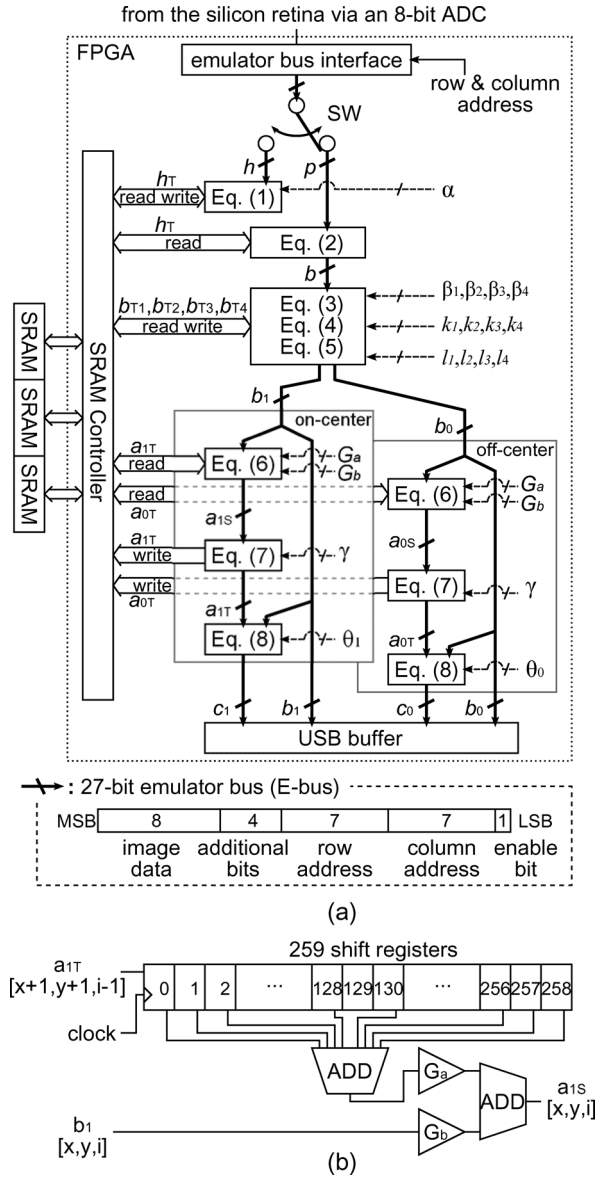

Fig. 8. Block diagram of digital circuits synthesized in the FPGA. (a) Block diagram of the entire circuit in the FPGA. Blocks indicated by an equation number [(1) –(8)] represent computation modules that compute the equation expressed in Section II. Parameters coupled with a dotted arrow correspond to the ones used in Section II equations. Thick arrows connecting computation modules represent the emulator bus (E-bus), the format of which is shown at the bottom of the figure. (b) Block diagram that performs spatial filtering in a single clock cycle. This circuit is used in (6) computation module.

The image data are converted into 8-bit digital data and are arranged according to the emulator bus (E-bus) format shown at the bottom of Fig. 8(a). It is composed of the input data (8 bits), additional bits (4 bits), row address (7 bits), column address (7 bits), and an enable bit. The enable bit is asserted for a single clock cycle when the E-bus interface [at the top of Fig. 8(a)] receives a new pixel value.

All modules of the FPGA operate at 40 MHz. Computation modules, indicated by an equation number, are connected to the E-bus. Fig. 9 shows the block diagram and time chart of

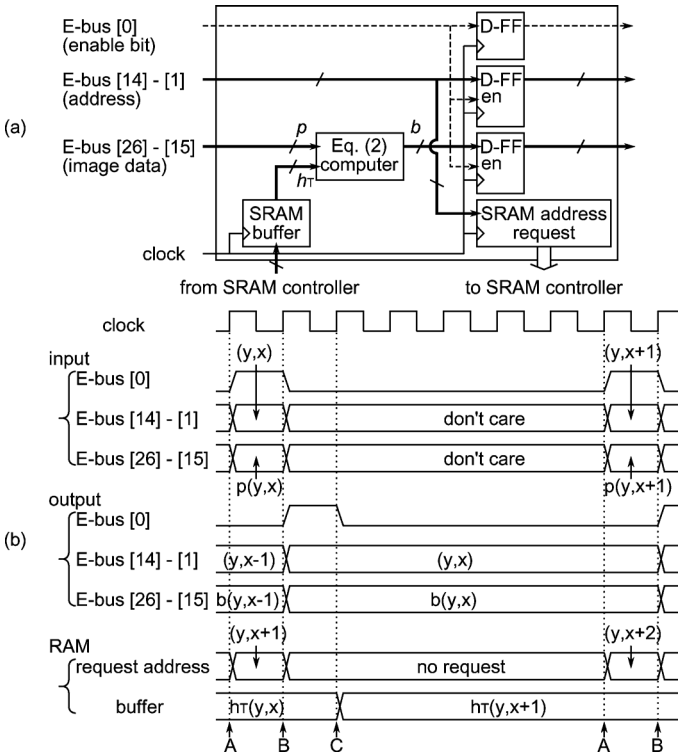

Fig. 9. Circuit diagram and time chart of (2) computation module. (a) Circuit diagram. The block indicated by DFF is a D-type flip-flop. Terminal "en" represents the enable input. (b) Time chart. See text for details.

a computation module. Although the block diagram and time chart of computation module (2) are shown in the figure as an example, those of other computation modules are essentially identical. The block indicated by (2) computer in Fig. 9(a) is a logic block that computes (2). It receives a new pixel value at time A in Fig. 9(b), and outputs the result within a single clock cycle. The result and address are passed to the next computation module when the enable bit of the input E-bus is high [at time B in Fig. 9(b)]. At the same, this module accesses the static random-access memory (SRAM) location in reference to the address information in the E-bus. To minimize the computation delay, a read request is sent to the SRAM [at time A in Fig. 9(b)] and the data is received [at time C in Fig. 9(b)] prior to the acquisition of the next pixel value. Computation modules rely only on E-bus information and operate independently; therefore, they can be easily modified/added/deleted.

Fig. 8(b) shows the circuit diagram that performs the spatial filtering used in (6). To reduce the times that the memory is accessed, a shift register buffering data of two rows and three pixels is employed. With this circuit structure, accessing the memory only once suffices to complete the spatial filtering, provided the shift register stores the data required for the filtering of the preceding pixel.

The length of the additional bit was determined so that the rounding error of IIR filters is equal to or lower than one least significant bit (LSB) of the input data. Fig. 10 shows the difference between the impulse response of an IIR filter computed with 64-bit floating point and that computed with fixed point. The impulse response of the IIR filter is shown in the inset. This filter has the longest time constant considered in this study, and

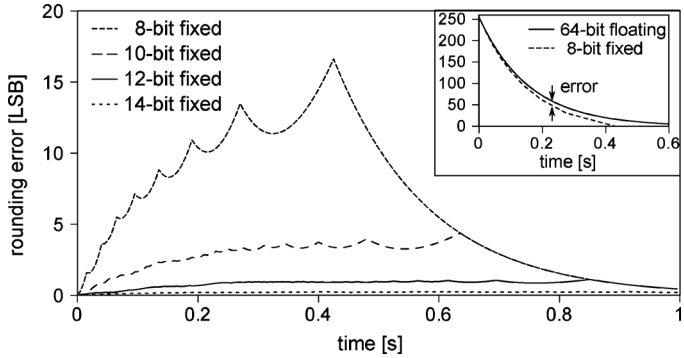

Fig. 10. Rounding error of an IIR filter computed with fixed point. The inset shows the impulse response of the IIR filter.

its value decreases to half of its initial value at 110 ms. The filter coefficient, which corresponds to α in (1) or β_n in (3), is 0.031. We chose the 12-bit fixed point because its maximum error is about 1 LSB. Using a 14-bit or greater bit fixed point would be ideal in terms of obtaining a negligible total simulated value error, provided the memory capacity and bandwidth allow it.

The SRAM controller controls three SRAMs whose data-bus width is 16 bits. The total capacity of the three SRAMs is 3 Mbits. Although 192 bits can be allocated to a single pixel, the accessible data are limited by the memory bandwidth. Because signal p comes every seven clock cycles, the maximum amount of accessible data for a single pixel is 336 bits ($3 \times 16 \times 7$). Assuming that the number of read and write requests is the same, the available memory size is 168 bits. The size of the memory used in this study is 84 bits. The remaining is reserved for other modules (e.g., spiking neuron modules) that will be installed in future works.

IV. Experiments

The output signal of the retina emulator was examined by presenting images on a liquid crystal display (LCD) as well as natural scenes. Images were presented on an LCD located at a distance of 30 cm from the emulator, which is equipped with a lens. The f-number of the lens was set to 1.4. Image acquisition and all computations were completed in this emulator, and its simulated potentials were sent to a PC for recording.

The following three movies were used in this study: a movie in which a stationary white spot appeared and disappeared on a black background, a movie in which a white spot moved at a uniform velocity and stopped on a black background, and a movie in which a white spot was occluded by a black rectangle on a gray background. These three movies were selected because appearance, motion, and occlusion are fundamental components that form natural scenes. The luminance of the white, black, and gray areas is 142 $\mathrm{cd/m^2}$, 1.8 $\mathrm{cd/m^2}$, and 22 $\mathrm{cd/m^2}$, respectively.

The parameter values used in this experiment are listed in Table I. The spatial and temporal properties of the OPL reproduced with these parameters are shown in Figs. 5 and 6(a) (dashed line), respectively. The time to peak for bipolar cells is 70 ms. In this section, we will show simulated graded potentials on the sustained on-center pathway (b_1 in Fig. 4) and the transient on-center and off-center pathways (c_1 and c_0 in Fig. 4).

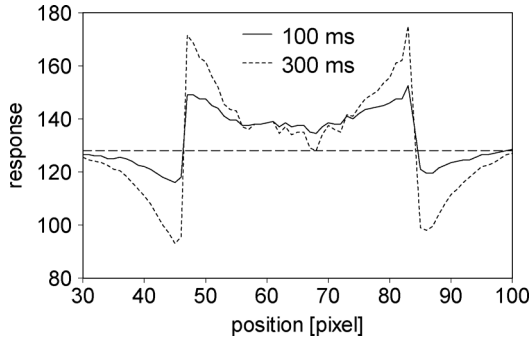

Fig. 11. Profiles of the simulated potentials on the sustained on-center pathway at the 64th row. The solid and dotted lines plot potentials at 100 ms and 300 ms, respectively, after the appearance of a spot. The horizontal dashed line represents the resting potential ($= 128$).

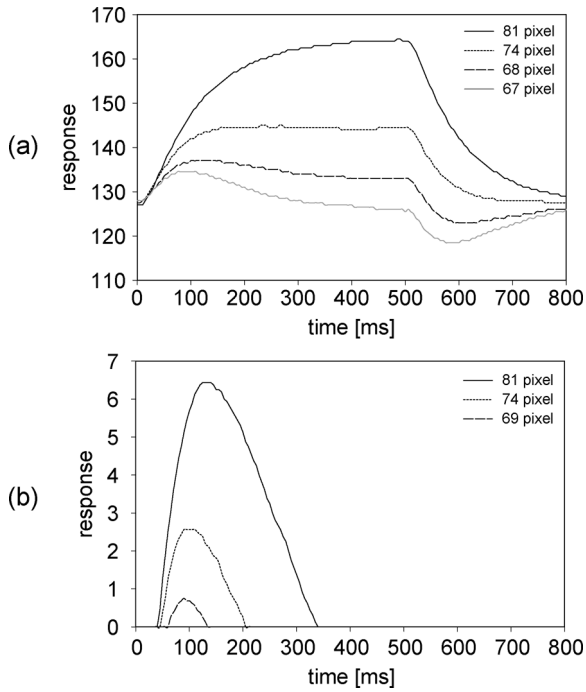

Fig. 12. Time courses of the simulated potentials of the on-center pathway at 5 points at the 64th row. A white spot whose contours were on pixels 46 and 84 appeared at 0 ms and disappeared at 500 ms. (a) Potentials on the sustained on-center pathway (b_1 in Fig. 4). (b) Potentials on the transient on-center pathway (c_1 inFig. 4).

A. Responses to a Stationary White Spot

A stationary white spot was displayed for 500 ms on an LCD. On the silicon retina chip, the spot was 38 pixels in diameter, and its contour at the 64th row was on the 46th and the 84th pixels.

Fig. 11 shows simulated sustained responses of the 64th row at 100 ms and 300 ms after the appearance of the spot, respectively. The whole area in the spot responded at first as shown by the solid line whereas the center region was suppressed by delayed lateral inhibition at 300 ms after the appearance as shown by the dotted line. Consequently, the region around the contour was strongly enhanced. This fact indicates that edge enhancement should require hundreds of milliseconds.

Fig. 12(a) and (b) shows the time courses of potentials on the sustained and transient on-center pathways, respectively. The type of plotted line indicates the position at the 64th row, as shown in the legend. The peak amplitude and the rate of increase in the potential on the sustained pathway depended on the distance from the contour. In addition, the shape of the time course on the sustained pathway also depended on the distance from the contour: the cells near the contour exhibited a simple low-pass-type response, whereas those at a short distance away from the contour (68th pixel in Fig. 12) exhibited a response with a peak and plateau. These dependencies on the distance from the contour were caused by the delayed inhibition mediated by horizontal cells. They directly affected the potential on the transient pathway, whose peak amplitude and delay also depended on the distance from the contour.

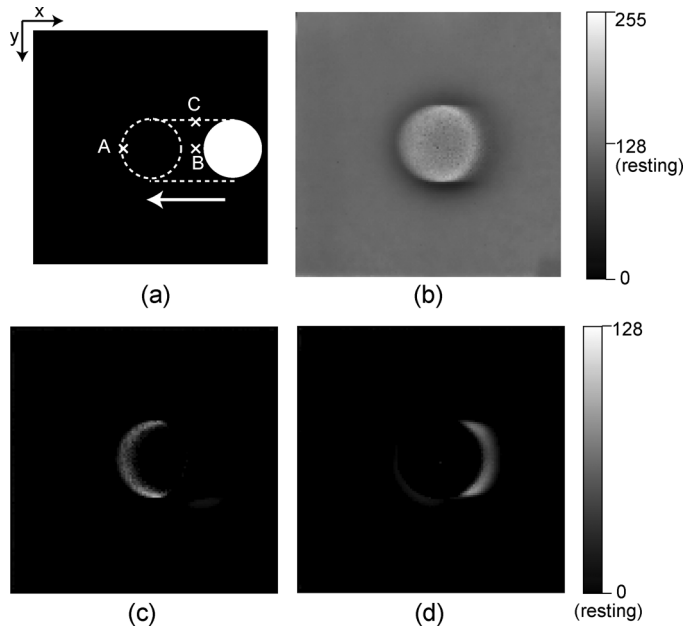

Fig. 13. Input image and simulated potentials in response to a white spot in motion. (a) Movie used as the visual stimulus. A white circle moves leftward at 0.22 pixels/frame and stops at the center of the view. Dashed lines indicate the trajectory of the contour and the position where the circle stops. Crosses with letters indicate the positions at which the simulated neural responses presented in Fig. 14. The coordinates (x, y) for points A, B, and C are (47, 62), (96, 62), and (96, 46), respectively. Here, the coordinates for the top left corner are (0, 0), and those for the bottom right corner are (127, 127). Point A is inside of the circle after it stops. Point C is inside of the trajectory. (b), (c), and (d) Spatial pattern of simulated potentials at -10 ms in Fig. 14. The bar with a gray-scale gradation on the right side of each row represents the potential. (b) Simulated potentials on the sustained on-center pathway (b_1 in Fig. 4). The value 128 indicates the resting potential. (c) and (d) Simulated potentials on the transient on-center (c) and off-center (d) pathways (c_1 and c_0, respectively, in Fig. 4). The value 0 indicates the resting potential.

B. Responses to a Moving White Spot

A white spot moving leftward and stopping at the center of the field of view was displayed on an LCD, as shown in Fig. 13(a). On the silicon retina chip, the diameter of the spot is the same as that used in the previous experiment.

Fig. 13(b) shows a spatial pattern of simulated potentials on the sustained on-center pathway in response to a spot in motion. Cells around the contour exhibited a higher response; in particular, cells near the top and bottom of the contour responded strongly because cells in these areas receive input from the contour for a longer duration. This result can be seen in detail from the plot of the time course for on-center cells at

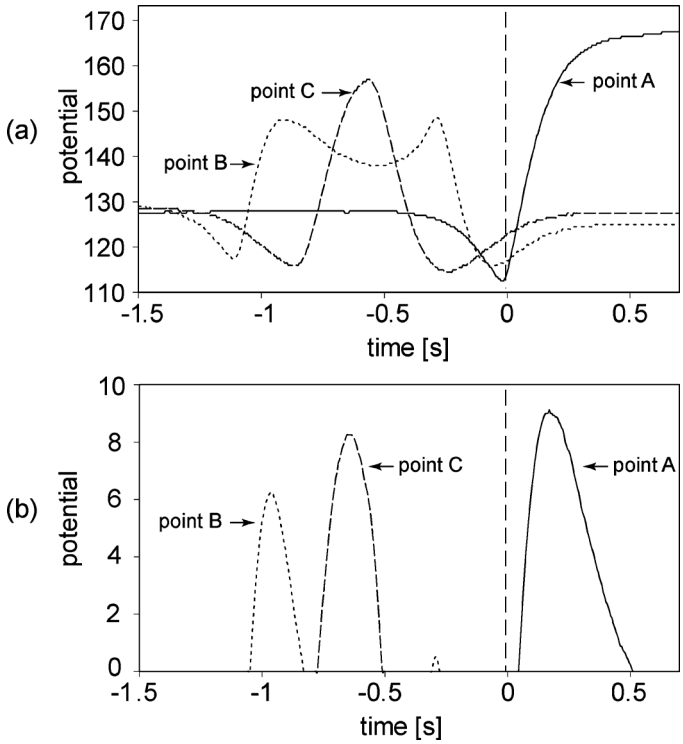

Fig. 14. Time courses of simulated potentials on the (a) sustained and (b) transient on-center pathways (b_1 and c_1, respectively, in Fig. 4) at the points indicated in Fig. 13(a). The vertical dashed line indicates the time when the circle stopped.

point C [Fig. 14(a)]. This result indicates that the trajectory of both sides of a moving object is enhanced in the retina.

The time courses [Fig. 14(a)] also show that the amplitude of the potential at a point where the circle passed through was much weaker than that at a point where the contour of the circle stopped. This difference in amplitude was also caused by the difference in input duration.

Fig. 13(c) and (d) shows the spatial patterns of simulated potentials on the transient on-center and off-center pathways, respectively, in response to a spot in motion. On-center cells exhibited a stronger response to the preceding edge, whereas off-center cells responded strongly to the following edge.

The time courses of the response of the transient pathway [Fig. 14(b)] also show that the cells around the contour exhibited the highest response with a particular delay after the circle stopped. In this experiment, the response of on-center cells reached their maximum value with a delay of 170 ms.

These results indicate that moving objects that stop in the field of view are enhanced after a certain delay in the retina.

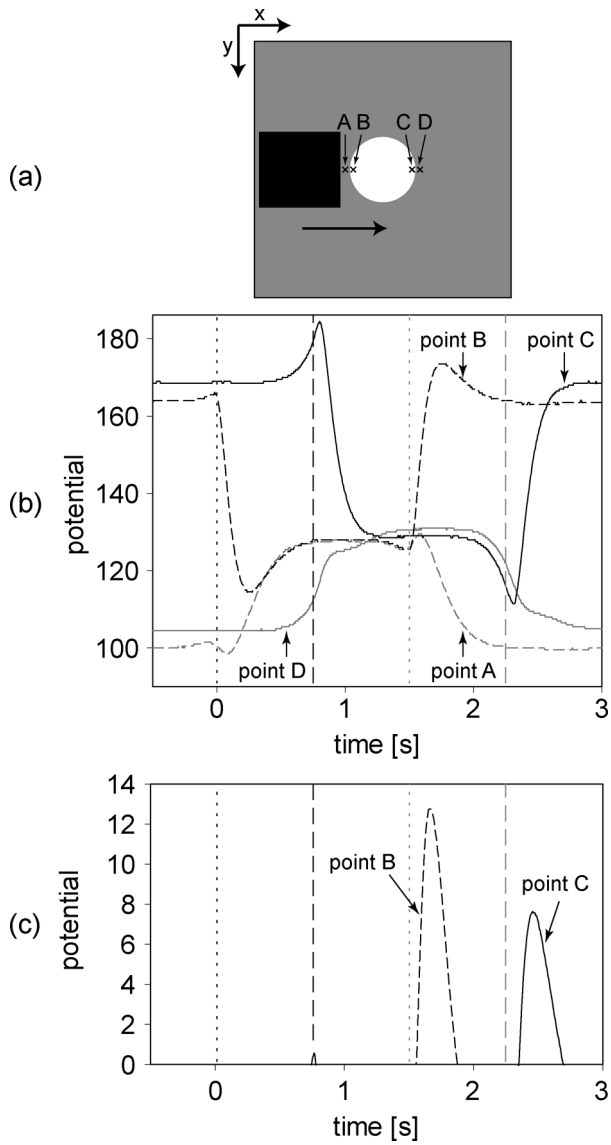

Fig. 15. Input image and simulated potentials in response to occlusion. (a) Movie used as the visual stimulus. A black rectangle moves rightward and hides a white circle on a gray background. This movie simulates a situation where one object occludes another, for example, when a person blinks. Crosses with letters indicate positions at which the simulated neural responses presented in (b) and (c) were obtained. The coordinates of points A, B, C, and D are (44, 63), (47, 63), (82, 63), and (84, 63), respectively. Here, the coordinates are the same as those used in Fig. 13(a). Points A and D are outside of the circle, whereas Points B and C are inside of the circle. (b)(c) Time courses of simulated potentials at the points indicated in (a). The black dotted and dashed vertical lines indicate the times at which the left and right edges, respectively, of the circle were occluded by the rectangle. The gray dotted and dashed vertical lines indicate the times at which the left and right edges, respectively, of the circle reemerged. (b) Time courses of sustained on-center cells. (c) Time courses of transient on-center cells.

C. Responses to Occlusion

A movie in which a black rectangle moves rightward hiding a white circle on gray background [Fig. 15(a)] was displayed on an LCD. The diameter of the spot was again identical to that used in the previous experiment.

Fig. 15(b) and (c) shows the time courses of simulated potentials at the points indicated in Fig. 15(a). The left and right edges of the white circle were occluded by the black rectangle at 0 ms and 780 ms, respectively. They reemerged correspondingly at 1490 ms and 2260 ms.

Naturally, the potential of the sustained on-center pathway approached the resting potential (a value of 128) when the circle was occluded by the rectangle, and it returned to its initial potential when the circle reemerged [Fig. 15(b)]. In addition to this increase and decrease, the potentials at points B and C exhibited a response peak at their reappearance and disappearance,

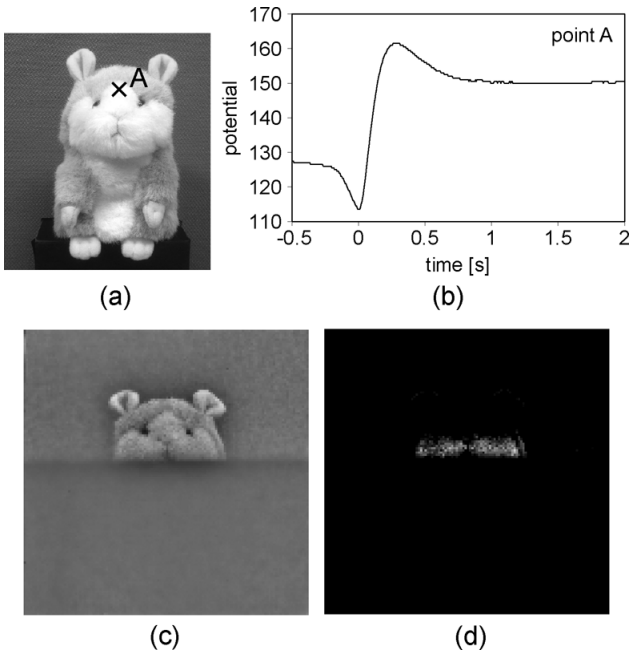

Fig. 16. Input scene and simulated potentials in room lighting. (a) Doll presented to examine results of emulating a real-world scene. The cross with the letter A indicates the position at which the simulated neural responses presented in (b) was obtained. (b) Time course of the graded potentials on the sustained on-center pathway at point A in (a). (c) and (d) Spatial patterns of simulated potentials of the sustained (c) and transient (d) on-center pathways in response to a doll in room lighting.

respectively, owing to a decrease in lateral inhibition; this decrease occurred because the circle around point B or C was occluded by the rectangle.

The peak response of the sustained pathway caused a large-peaked response at the reappearance of point B on the transient on-center pathway. Therefore, the peak amplitude at the reappearance of point B was much higher than that at the reappearance of point C.

D. Responses to a Doll in Room Lighting

Graded potentials in response to a real-world scene were examined by presenting a doll [Fig. 16(a)] in room lighting. The doll was hidden by a sheet of black paper and appeared from head to toe.

Fig. 16(c) shows the spatial patterns of simulated potentials on the sustained on-center pathway. The lower half of the doll was still hidden at this point. Naturally, cells around contours with a high contrast responded strongly. In addition, cells around contours exhibited a higher potential at the appearance of the contour for the same reason as that described in the previous section. This result is seen in detail in the time course of the potentials [Fig. 16(b)].

Fig. 16(d) shows the spatial patterns of simulated potentials on the transient on-center pathway. Because the transient cells code essentially the temporal change of the sustained cells, they responded to only a part of the doll just after its appearance. Therefore, a small segment was presented in Fig. 16(d).

The result is also shown in a supplementary movie file. The movie was slowed down to 30 fps for easier viewing while the real processing speed was 200 fps.

V. Discussion

In this section, the following topics are discussed: interpretations and usage of emulated response (Sections A and B), sampling rate required for emulation of the retina (Section C), appropriate architecture for emulation of the retina (Sections D and E), and future improvements of the emulator (Section F).

A. Possible Interpretations of Emulated Response

In the present study, we emulated the responses of retinal neurons to a few simple situations: motion and occlusion. How do these responses contribute to our perception in natural situations?

Simulated neurons exhibited a strong short-term response to a moving circle after it stopped, whereas the response to a circle in motion was suppressed by low-pass temporal filtering (Fig. 14). Responses to an object moving quickly would be suppressed strongly. This property would useful for suppressing rapidly moving images reflected on the retina during saccadic eye movements. In addition, it could emphasize images immediately after saccadic eye movements, and hence help us quickly perceive the surrounding environment.

Simulated neurons exhibited a response peak just before and after occlusion (Fig. 15). This property can emphasize an hiding and emerging object, which could be a threat for animals. It shows another aspect when we consider blinks, which cause occlusion of an entire visual field. The peak response with a short rise time could help us perceive the surrounding environment quickly.

B. Usage of the Retina Emulator

This emulator can help advance studies on the retina in various situations. First, it suggests different functional roles for particular sub-circuits of the retina under natural conditions. It also provides a useful simulation environment to develop and verify physiological models of the retina. To develop a physiological model, comparing intracellular recordings obtained by a physiological experiment with the response emulated by the model is helpful. In particular, the emulator is effective when a natural scene is used as a visual stimulus because the neuronal responses to such scenes cannot be predicted easily from the receptive field measured with simple stimuli in intracellular recordings. Therefore, an emulated response could be a good reference.

Furthermore, the emulated results can be compared directly with the results of psychophysical experiments because the emulator can generate retinal responses in the same visual environments as those designed for human subjects. The psychophysical experiments carried out by de Lange [40] and Kelly [41] have revealed that the human visual system also exhibits low-pass temporal filtering. If the model parameters are determined on the basis of physiological data from the primate retina, a quantitative comparison of the psychophysical data with the emulated results in this study would be possible.

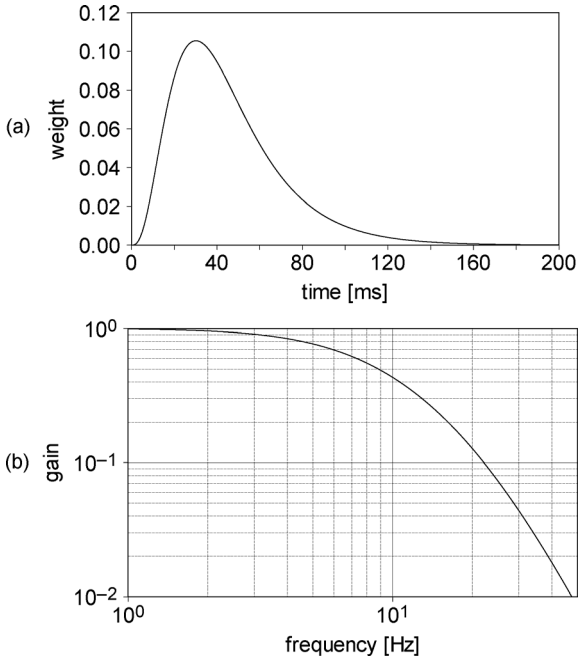

Fig. 17. Time course and frequency-gain relationship of the response of a photoreceptor modeled by Baylor *et al.* [42].

C. Is 200 Hz Sampling Appropriate?

What sampling rate is required to reproduce the graded potentials of retinal neurons accurately? The answer to this question is intimately related to the temporal frequency characteristics of the photoreceptor response because all graded potentials are generated from the photoreceptor response. To emulate the retinas of various vertebrates, the sampling rate must be sufficient to reproduce the temporal characteristics of fast-responding photoreceptors among vertebrates. The response of a photoreceptor to a flash of light can be approximated by the following equation: [42]

$$U = exp(-\alpha t)\{1 - exp(-\alpha t)\}^{(n-1)}. \tag{9}$$

Although this equation was devised to express the response of a photoreceptor in the turtle, we approximate the response of a monkey photoreceptor by substituting an appropriate value of α. The time to peak for photoreceptors in the monkey is as short as 30 ms when they are dark-adapted [43]. Substituting $\alpha = 46\ \mathrm{s}^{-1}$ and $\mathrm{n} = 4$ into (9), we obtain a time course whose time to peak is 30 ms, as shown in Fig. 17(a). Fig. 17(b) shows its amplitude spectrum normalized by dividing by the value at 1 Hz. The amplitude decreases greatly at higher frequencies; for example, it declines to 1/10 at 22 Hz. Therefore, a sampling rate of 200 Hz has little effect on the filter that simulates the temporal property of a photoreceptor.

D. Mixed Analog-Digital Architecture

We developed a retina emulator that uses a mixed analog-digital architecture to take advantage of both analog circuits, which perform specific computations instantaneously with low power dissipation, and digital systems, which are programmable and scalable. Both advantages play important roles in simulating the complex activities of retinal neurons in real time (Section V.E). This emulator, which reproduces neural activity in the retina in real time and has many configurable parameters (Table I), could be an useful tool because it enables researchers to examine the neural activities in response to natural scenes under natural conditions simulated with various parameters.

In a previous study, another analog silicon retina [44] was employed as the input device of a retinal simulation performed in MATLAB [45]. This silicon retina generates spikes whose frequency codes the rate of temporal change in luminance, and a software program written in MATLAB applies spatio-temporal filters to the spike image. However, reproducing physiologically feasible graded potentials from trains of such spikes in real time is difficult. This is because the spikes do not directly code the time course of light intensity required to reproduce the neuronal response of photoreceptors and because the spatio-temporal filters required to reproduce the potential was implemented by a software program.

It is highly important to elaborate on an architecture that takes advantage of analog and digital systems, so that the spatio-temporal processing required for retinal simulations is performed efficiently.

E. Emulating Spatio-Temporal Properties of the Retina

That retinal neurons (in particular, horizontal cells) are laterally interconnected and that visual signals spread widely are well-known facts. Examining the effect of the spatial properties of lateral spread requires a wide spatial filter with configurable spatial properties. While mismatch, a common issue with analog circuits, has some effect on the result, an analog resistive network of MOS transistors is suitable for this purpose because of its configurability and instantaneous computation of wide spatial filtering.

The temporal properties of retinal neurons were simulated in a digital system because analog integrated circuits are not suitable for implementing accurate and configurable temporal filters with a long time constant of neurons. IIR filters were employed to conserve memory capacity. Although the shapes of the weight function of IIR filters are limited to several types in contrast to those of finite infinite response (FIR) filters, which are totally configurable, the combination of multiple IIR filters can form weight functions that simulate neural activities (Fig. 6). Therefore, this emulator can be used to examine the temporal properties of retinal neurons.

Although a temporal shift function would be required to reflect a synaptic delay, such a function is not incorporated in the retina emulator developed in this study owing to inadequate memory capacity and bandwidth. We will include this function in the next step by using a random access memory with adequate capacity and bandwidth.

F. Future Improvement of the IPL Model

In the present study, we implemented a simplified IPL model to reproduce responses for convenience. Although the present emulator suggested several interesting aspects of retinal responses, the model should be elaborated to reproduce retinal responses with greater accuracy. In addition, models of other

sub-circuits should be incorporated to obtain diverse retinal responses. By taking advantage of our extensible architecture, the neuronal circuit model in the emulator can easily be extended or modified.

Incorporating models of various sub-circuits in the IPL mediated by a wide variety of amacrine cells is also important to speculate about or verify their functional roles. For example, a neuronal circuit expected to eliminate the effect of fixational movement has recently been proposed on the basis of physiological experiments [46]. This emulator could verify such a function under natural conditions [47].

Generating a physiologically feasible spike train is also one of the next most important steps. Because several types of spike patterns have been found in ganglion cells, a spiking model capable of generating multiple spike patterns, such as the Izhikevich model [48], would be required to reproduce a variety of spiking patterns.

REFERENCES

[1] G. Svaetichin, "The cone action potential," *Acta Phys. Scand.*, vol. 29, pp. 565–600, 1953, Suppl. 106.

[2] T. Tomita, "Electrophysiological study of the mechanisms subserving color coding in the fish retina," in *Proc. Cold Spring Harbor Symp. Quantitative Biology*, 1965, vol. 30, pp. 559–566.

[3] J. E. Dowling, *The Retina: An Approachable Part of the Brain*, 1st ed. Cambridge, MA, USA: Belknap Press (Harvard Univ. Press), 1987.

[4] D. A. Baylor, "Photoreceptor signals and vision. Proctor lecture," *Invest. Ophthal. Vis. Sci.*, vol. 28, no. 1, pp. 34–49, Jan. 1987.

[5] F. S. Werblin and J. E. Dowling, "Organization of the retina of the mudpuppy, necturus maculosus. II. Intracellular recording," *J. Neurophysiol.*, vol. 32, no. 3, pp. 339–355, May 1969.

[6] R. W. Rodieck, *The First Steps in Seeing*. Sunderland, MA, USA: Sinauer Assoc., 1998.

[7] J. Teeters, A. Jacobs, and F. Werblin, "How neural interactions form neural responses in the salamander retina," *J. Comput. Neurosci.*, vol. 4, no. 1, pp. 5–27, 1997.

[8] M. H. Hennig, K. Funke, and F. Worgotter, "The influence of different retinal subcircuits on the nonlinearity of ganglion cell behavior," *J. Neurosci.*, vol. 22, no. 19, pp. 8726–8738, Jan. 2002.

[9] A. Thiel, M. Greschner, and J. Ammermuller, "The temporal structure of transient ON/OFF ganglion cell responses and its relation to intraretinal processing," *J. Comput. Neurosci.*, vol. 21, no. 2, pp. 131–151, 2006.

[10] T. Gollisch and M. Meister, "Modeling convergent ON and OFF pathways in the early visual system," *Biol. Cybern.*, vol. 99, no. 4-5, pp. 263–278, Nov. 2008.

[11] C. A. Mead and M. Mahowald, "A silicon model of early visual processing," *Neural Netw.*, vol. 1, no. 1, pp. 91–97, 1988.

[12] C. Mead, "Neuromorphic electronic systems," *Proc. IEEE*, vol. 78, no. 10, pp. 1629–1636, 1990.

[13] G. Indiveri and R. Douglas, "Neuromorphic vision sensors," *Science*, vol. 288, no. 5469, pp. 1189–1190, May 2000.

[14] S. Liu and T. Delbruck, "Neuromorphic sensory systems," *Current Opin. Neurobiol.*, vol. 20, no. 3, pp. 288–295, Jun. 2010.

[15] P. Chung-Yu Wu and C.-F. Chiu, "A new structure of the 2-d silicon retina," *IEEE J. Solid-State Circuits*, vol. 30, no. 8, pp. 890–897, 1995.

[16] K. A. Boahen and A. G. Andreou, "A contrast sensitive silicon retina with reciprocal synapses," *Adv. Neural Inf. Process. Syst.*, vol. 4, pp. 764–772, 1991.

[17] H. Ikeda, K. Tsuji, T. Asai, H. Yonezu, and J.-K. Shin, "A novel retina chip with simple wiring for edge extraction," *IEEE Photon. Technol. Lett.*, vol. 10, no. 2, pp. 261–263, 1998.

[18] K. Zaghloul and K. Boahen, "Optic nerve signals in a neuromorphic chip I: Outer and inner retina models," *IEEE Trans. Biomed. Eng.*, vol. 51, no. 4, pp. 657–666, 2004.

[19] K. Zaghloul and K. Boahen, "Optic nerve signals in a neuromorphic chip II: Testing and results," *IEEE Trans. Biomed. Eng.*, vol. 51, no. 4, pp. 667–675, 2004.

[20] L.-J. Lin, P. Chung-Yu Wu, B. Roska, F. Werblin, D. Balya, and T. Roska, "A neuromorphic chip that imitates the ON brisk transient ganglion cell set in the retinas of rabbits," *IEEE Sensors J.*, vol. 7, no. 9, pp. 1248–1261, 2007.

[21] T. Delbruck and S.-C. Liu, "A silicon early visual system as a model animal," *Vis. Res.*, vol. 44, no. 17, pp. 2083–2089, Aug. 2004.

[22] B. Shi, "A low-power orientation-selective vision sensor," *IEEE Trans. Circuits Syst. II, Analog Digit. Signal Process.*, vol. 47, no. 5, pp. 435–440, 2000.

[23] R. Etienne-Cummings, J. Van der Spiegel, and P. Mueller, "A focal plane visual motion measurement sensor," *IEEE Trans. Circuits Syst. I, Fundam. Theory Appl.*, vol. 44, no. 1, pp. 55–66, 1997.

[24] R. Etienne-Cummings, J. Van der Spiegel, P. Mueller, and M.-Z. Zhang, "A foveated silicon retina for two-dimensional tracking," *IEEE Trans. Circuits Syst. II, Analog Digit, Signal Process.*, vol. 47, no. 6, pp. 504–517, 2000.

[25] D.-S. Park, J.-H. Kim, H.-S. Kim, J.-H. Park, J.-K. Shin, and M. Lee, "A foveated-structure CMOS retina chip for edge detection with local light adaptation," *Sens. Actuators A, Phys.*, vol. 108, no. 1–3, pp. 75–80, Nov. 2003.

[26] J. Costas-Santos, T. Serrano-Gotarredona, R. Serrano-Gotarredona, and B. Linares-Barranco, "A spatial contrast retina with on-chip calibration for neuromorphic spike-based AER vision systems," *IEEE Trans. Circuits Syst. I, Reg. Papers*, vol. 54, no. 7, pp. 1444–1458, 2007.

[27] Z. Fu, T. Delbruck, P. Lichtsteiner, and E. Culurciello, "An address-event fall detector for assisted living applications," *IEEE Trans. Biomed. Circuits Syst.*, vol. 2, no. 2, pp. 88–96, Jun. 2008.

[28] R. Serrano-Gotarredona, M. Oster, P. Lichtsteiner, A. Linares-Barranco, R. Paz-Vicente, F. Gomez-Rodriguez, L. Camunas-Mesa, R. Berner, M. Rivas-Perez, T. Delbruck, S.-C. Liu, R. Douglas, P. Hafliger, G. Jimenez-Moreno, A. Civit Ballcels, T. Serrano-Gotarredona, A. J. Acosta-Jimenez, and B. Linares-Barranco, "CAVIAR: A 45 k neuron, 5 M synapse, 12 G connects/s AER hardware sensory-processing- learning-actuating system for high-speed visual object recognition and tracking," *IEEE Trans. Neural Netw.*, vol. 20, no. 9, pp. 1417–1438, Sep. 2009.

[29] H. Okuno and T. Yagi, "Image sensor system with bio-inspired efficient coding and adaptation," *IEEE Trans. Biomed. Circuits Syst.*, vol. 6, no. 4, pp. 375–384, Aug. 2012.

[30] C. Zamarreno-Ramos, A. Linares-Barranco, T. Serrano-Gotarredona, and B. Linares-Barranco, "Multicasting mesh AER: A scalable assembly approach for reconfigurable neuromorphic structured AER systems. Application to ConvNets," *IEEE Trans. Biomed. Circuits Syst.*, vol. 7, no. 1, pp. 82–102, Feb. 2013.

[31] J. Hasegawa and T. Yagi, "Real-time emulation of neural images in the outer retinal circuit," *J. Physiol. Sci.*, vol. 58, no. 7, pp. 507–514, 2008.

[32] J. Hasegawa and T. Yagi, "Real-time emulation of dynamic features of sustained and transient channels in vertebrate retina," in *Proc. IEEE Biomedical Circuits and Systems Conf.*, Nov. 2009, pp. 197–200.

[33] S. Kameda and T. Yagi, "An analog VLSI chip emulating sustained and transient response channels of the vertebrate retina," *IEEE Trans. Neural Netw.*, vol. 14, no. 5, pp. 1405–1412, 2003.

[34] T. D. Lamb and E. J. Simon, "The relation between intercellular coupling and electrical noise in turtle photoreceptors," *J. Physiol.*, vol. 263, no. 2, pp. 257–286, Jan. 1976.

[35] K. I. Naka and W. A. H. Rushton, "The generation and spread of s-potentials in fish (cyprinidae)," *J. Physiol.*, vol. 192, no. 2, pp. 437–461, Jan. 1967.

[36] K. Shimonomura, S. Kameda, A. Iwata, and T. Yagi, "Wide-dynamic range APS-based silicon retina with brightness constancy," *IEEE Trans. Neural Netw.*, vol. 22, no. 9, pp. 1482–1493, 2011.

[37] A. Kaneko, "Physiological and morphological identification of horizontal, bipolar and amacrine cells in goldfish retina," *J. Physiol.*, vol. 207, no. 3, pp. 623–633, May 1970.

[38] T. Yagi, S. Ohshima, and Y. Funahashi, "The role of retinal bipolar cell in early vision: An implication with analogue networks and regularization theory," *Biol. Cybern.*, vol. 77, no. 3, pp. 163–171, Sep. 1997.

[39] S. Ohshima, T. Yagi, and Y. Funahashi, "Computational studies on the interaction between red cone and h1 horizontal cell," *Vis. Res.*, vol. 35, no. 1, pp. 149–160, Jan. 1995.

[40] H. De Lange Dzn, "Research into the dynamic nature of the human fovea-cortex systems with intermittent and modulated light. I. Attenuation characteristics with white and colored light," *J. Opt. Soc. Amer.*, vol. 48, no. 11, pp. 777–784, Nov. 1958.

[41] D. H. Kelly, "Visual responses to time-dependent stimuli. I. Amplitude sensitivity measurements," *J. Opt. Soc. Amer.*, vol. 51, no. 4, pp. 422–429, Apr. 1961.
[42] D. A. Baylor, A. L. Hodgkin, and T. D. Lamb, "The electrical response of turtle cones to flashes and steps of light," *J. Physiol.*, vol. 242, no. 3, pp. 685–727, Nov. 1974.
[43] D. M. Schneeweis and J. L. Schnapf, "The photovoltage of macaque cone photoreceptors: Adaptation, noise, and kinetics," *J. Neurosci.*, vol. 19, no. 4, pp. 1203–1216, Feb. 1999.
[44] P. Lichtsteiner, C. Posch, and T. Delbruck, "A 128 × 128 120 dB 15 μs latency asynchronous temporal contrast vision sensor," *IEEE J. Solid-State Circuits*, vol. 43, no. 2, pp. 566–576, 2008.
[45] H. Lorach, R. Benosman, O. Marre, S.-H. Ieng, J. A. Sahel, and S. Picaud, "Artificial retina: The multichannel processing of the mammalian retina achieved with a neuromorphic asynchronous light acquisition device," *J. Neural Eng.*, vol. 9, no. 6, p. 066004, Dec. 2012.
[46] S. A. Baccus, B. P. Olveczky, M. Manu, and M. Meister, "A retinal circuit that computes object motion," *J. Neurosci.*, vol. 28, no. 27, pp. 6807–6817, Jul. 2008.
[47] J. Hasegawa and T. Yagi, "Emulation of retinal cell responses during fixational eye movements," *IEICE Electron. Expr.*, vol. 7, no. 3, pp. 184–189, 2010.
[48] E. M. Izhikevich, "Simple model of spiking neurons," *IEEE Trans. Neural Netw.*, vol. 14, no. 6, pp. 1569–1572, Nov. 2003.

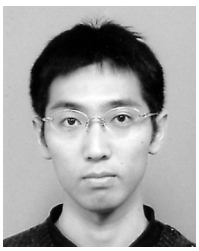

Hirotsugu Okuno received the Ph.D. degree in electrical, electronic, and information engineering from Osaka University, Osaka, Japan, in 2008.

Currently, he is an Assistant Professor at the Graduate School of Engineering, Osaka University. His research interests include visual signal processing in biological systems and their applications in robotics.

Jun Hasegawa received the Ph.D. degree in electrical, electronic, and information engineering from Osaka University, Osaka, Japan, in 2010.

Currently, he works for MIRAIT Information Systems Company Ltd., Osaka, Japan. His interests include visual signal processing in biological systems and their applications in computer vision systems.

Tadashi Sanada is currently working toward the Ph.D. degree in the Division of Electrical, Electronic and Information Engineering, Osaka University, Osaka, Japan. His research interests include visual information processing in biological systems, neural image simulation, and spiking neural networks.

Tetsuya Yagi received the Ph.D. degree in medical science from Nagoya University, Nagoya, Japan, in 1985.

Following his studies as a Postdoctoral Fellow with the National Institute of Physiological Science and Rockefeller University, he joined the Kyushu Institute of Technology as an Associate Professor in 1990. Currently, he is a Professor with the Graduate School of Engineering, Osaka University, Osaka, Japan. His research interests include neurophysiology of visual systems and neuromorphic engineering systems.